Journal of Hazardous Materials 196 (2011) 255–262

Contents lists available at SciVerse ScienceDirect

Journal of Hazardous Materials

journal homepage: www.elsevier.com/locate/jhazmat

Enhanced photocatalytic activity of Bi_2WO_6 with oxygen vacancies by zirconium doping

Zhijie Zhang, Wenzhong Wang*, Erping Gao, Meng Shang, Jiehui Xu

State Key Laboratory of High Performance Ceramics and Superfine Microstructures, Shanghai Institute of Ceramics, Chinese Academy of Sciences, 1295 Dingxi Road, Shanghai 200050, PR China

ARTICLE INFO

Article history:
Received 3 July 2011
Received in revised form 5 September 2011
Accepted 6 September 2011
Available online 10 September 2011

Keywords:
Zr^{4+}-doped Bi_2WO_6
Oxygen vacancy
Photocatalysis
RhB
Phenol

ABSTRACT

To overcome the drawback of low photocatalytic efficiency brought by electron–hole recombination, Bi_2WO_6 photocatalysts with oxygen vacancies were synthesized by zirconium doping. The oxygen vacancies as the positive charge centers can trap the electron easily, thus inhibiting the recombination of charge carriers and prolonging the lifetime of electron. Moreover, the formation of oxygen vacancies favors the adsorption of O_2 on the semiconductor surface, thus facilitating the reduction of O_2 by the trapped electrons to generate superoxide radicals, which play a key role in the oxidation of organics. Visible-light-induced photodegradation of rhodamine B (RhB) and phenol were carried out to evaluate the photoactivity of the products. The results showed that oxygen-deficient Bi_2WO_6 exhibited much enhanced photoactivity than the Bi_2WO_6 photocatalyst free of oxygen deficiency. This work provided a new concept for rational design and development of high-performance photocatalysts.

1. Introduction

Semiconductor-based photocatalysis has been attracting a great deal of attention due to its potential applications in renewable energy and environment fields such as dye-sensitized solar cells, hydrogen generation from water splitting and photocatalytic water/air purification [1–5]. Because these applications are based on the photogeneration of charge carriers such as electrons and holes, success in the applications relies on the transfer efficiency of electron or hole, which is closely related to the recombination rates of the photogenerated charge carriers. Unfortunately, due to the much faster recombination rate (nanoseconds) than the interfacial transfer rate (microseconds to milliseconds), many charge carriers recombine and dissipate the input energy as heat, which seriously limits the overall quantum efficiency for photocatalysis [6]. Therefore, to improve the photocatalytic activity of the semiconductors, it is important to control the recombination dynamics of the photogenerated charge carriers. If a suitable scavenger or surface defect state is available to trap the electron or hole, recombination is inhibited and ensuing redox reaction may occur. It was reported that oxygen vacancies may act as electron capture centers, and thus play an important role in retarding the recombination of charge carriers, which can lead to an enhanced photocatalytic activity of the photocatalysts [7–9]. Moreover, the existing oxygen vacancies can act importantly as specific reaction sites for reactant molecules in heterogeneous reactions [10]. Therefore, introducing oxygen vacancies into the photocatalysts can be a feasible approach for developing highly active photocatalysts.

As one of the simplest Aurivillius oxides with layered structure, Bi_2WO_6 has recently attracted considerable attention for its good photocatalytic performance in water splitting and organic contaminant decomposing under visible light irradiation [11–15]. Up to now, much work has been done to facilitate the electron–hole separation and enhance the photocatalytic activity of Bi_2WO_6, including surface modification [16,17], anion doping [18], and coupling with other semiconductors [19,20]. However, to the best of our knowledge, the effect of oxygen vacancies on the photocatalytic activity of Bi_2WO_6 has seldom been reported.

Here for the first time we introduce oxygen vacancies into Bi_2WO_6 through zirconium doping and the relationship between oxygen vacancies and the photocatalytic activity of Bi_2WO_6 has been investigated. Bi_2WO_6 does not contain oxygen vacancies and it was reported that substitution of W by appropriate cations with lower valence states could lead to an extrinsic oxygen deficiency by charge compensation [21,22]. Defect calculations show that the low solution energy (0.05 eV) is favorable for the substitution of Zr^{IV} at W^{VI} site with the creation of extrinsic oxygen vacancies [22], which may be described by defect reactions written as:

$$ZrO_2 \xrightarrow{WO_3} Zr''_W + V_O^{\bullet\bullet} + 2O_O$$

In this study, we succeeded in preparing oxygen deficient Bi_2WO_6 phases by substitution for W^{VI} with Zr^{IV}. The photoactivity

* Corresponding author. Tel.: +86 21 5241 5295; fax: +86 21 5241 3122.
E-mail address: wzwang@mail.sic.ac.cn (W. Wang).

0304-3894/$ – see front matter © 2011 Elsevier B.V. All rights reserved.
doi:10.1016/j.jhazmat.2011.09.017

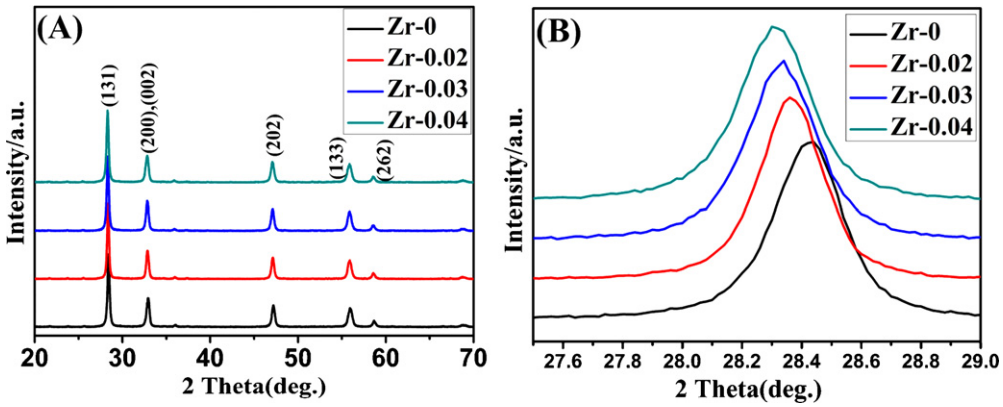

Fig. 1. (A) The XRD patterns of the as-synthesized products; (B) diffraction peak positions of the (1 3 1) plane in the range of $2\theta = 27.5–29^\circ$.

evaluation, via the photocatalytic degradation of RhB and phenol under visible light, demonstrated that the photocatalytic activity is dependent on the concentration of oxygen vacancy, and the Zr^{4+}-doped Bi_2WO_6 exhibit much better photocatalytic performance than undoped Bi_2WO_6 sample. Moreover, the role of oxygen vacancy in promoting the separation of charge carriers and enhancing the photocatalytic activities is elucidated in detail.

2. Experimental

2.1. Preparation of Zr^{4+}-doped Bi_2WO_6 photocatalysts

The Zr^{4+}-doped Bi_2WO_6 photocatalysts were prepared by a hydrothermal method. In a typical process, 2 mmol of $Bi(NO_3)_3{\cdot}5H_2O$ and 1 mmol of $Na_2WO_4{\cdot}2H_2O$ were dissolved in 2 mL of 2 M nitric acid and 30 mL of deionized water, respectively. After that, these two solutions were mixed together and stirred for 30 min. Then aqueous solution containing desired amounts of $ZrOCl_2{\cdot}8H_2O$ was added for Zr^{4+}-doped Bi_2WO_6. The molar ratios of Zr to Bi_2WO_6 were set as 0, 2.0%, 3.0% and 4.0%, respectively, and the corresponding products were named as Zr-0, Zr-0.02, Zr-0.03 and Zr-0.04. The pH value of the final suspension was adjusted to about 7 and the mixture was stirred for several hours at room temperature. Afterward, the suspensions were added into a 50 mL Teflon-lined autoclave up to 80% of the total volume. The autoclave was sealed in a stainless steel tank and heated at 160 °C for 24 h. Subsequently, the autoclave was cooled to room temperature naturally. The products were collected by filtration, washed with distilled water for several times, and then dried at 60 °C in air for 12 h.

2.2. Characterization

The phase and composition of the as-prepared samples were measured by X-ray diffraction (XRD) studies using an X-ray diffractometer with Cu Kα radiation under 40 kV and 100 mA and with the 2θ ranging from 20° to 60° (Rigaku, Japan). The morphologies and microstructures of the as-prepared samples were investigated by transmission electron microscopy (TEM, JEOL JEM-2100F). UV–vis diffuse reflectance spectra (DRS) of the samples were recorded with an UV–vis spectrophotometer (Hitachi U-3010) using $BaSO_4$ as reference. Chemical compositions of the derived products were analyzed using X-ray photoelectron spectroscopy (XPS) analysis (Thermo Scientific Escalab 250). All binding energies were referenced to the C 1s peak (284.8 eV) arising from adventitious carbon. The photoluminescence (PL) spectra of the samples were recorded with a Perkin Elmer LS55. Total organic carbon (TOC) analysis was carried out with an elementar liqui TOC II analyzer.

2.3. Photocurrent measurement

Photocurrent measurements were carried out by using a CHI 660C electrochemical workstation. 25 mg of photocatalyst was suspended in de-ionized water (50 mL) containing acetate (0.1 M) and Fe^{3+} (0.1 mM) as an electron donor and acceptor, respectively. A Pt plate (both sides exposed to solution), a saturated calomel electrode (SCE), and a Pt gauze were immersed in the reactor as working (collector), reference, and counter electrodes, respectively. Photocurrents were measured by applying a potential (+1 V vs SCE) to the Pt electrode using a potentiostat (EG&G).

2.4. Measurement of photocatalytic activities

Photocatalytic activities of the Zr^{4+}-doped Bi_2WO_6 photocatalysts were measured by monitoring photo-degradation of rhodamine B (RhB) and phenol in aqueous solution. 100 mg of the photocatalysts were dispersed in a 100 mL solution of RhB (10^{-5} mol/L) or phenol (20 mg/L). Before illumination, the suspensions were magnetically stirred in the dark for 1 h to ensure adsorption/desorption equilibrium of RhB or phenol with the photocatalyst powders, and then exposed to visible light from a 500 W Xe lamp with a 420 nm cutoff filter. After a certain period of irradiation, 3 mL suspension was sampled and centrifuged to remove the photocatalysts. After that, the supernatant was taken out to measure the absorption spectral change of RhB or phenol through a UV–vis spectrophotometer (Hitachi U-3010) to monitor the photodegradation rate. The concentration change of rhodamine B and phenol were determined by monitoring the optical intensity of absorption spectra at 553 nm and 270 nm, respectively.

3. Results and discussion

3.1. Crystal structure and morphology of the products

The XRD diffraction patterns of the pure Bi_2WO_6 and Zr^{4+}-doped Bi_2WO_6 samples are shown in Fig. 1(A). All of the diffraction peaks match the standard data for a Russellite Bi_2WO_6 structure (JCPDS 39-0256), and no characteristic peaks of any impurities are detected in the patterns, which demonstrates that doping with zirconium does not result in the development of new phases. However, a careful comparison of the (1 3 1) diffraction peaks in the range of $2\theta = 27.5–29^\circ$ (Fig. 1(B)) shows that the peak position of Bi_2WO_6 shifts slightly toward a lower 2θ value with the increase

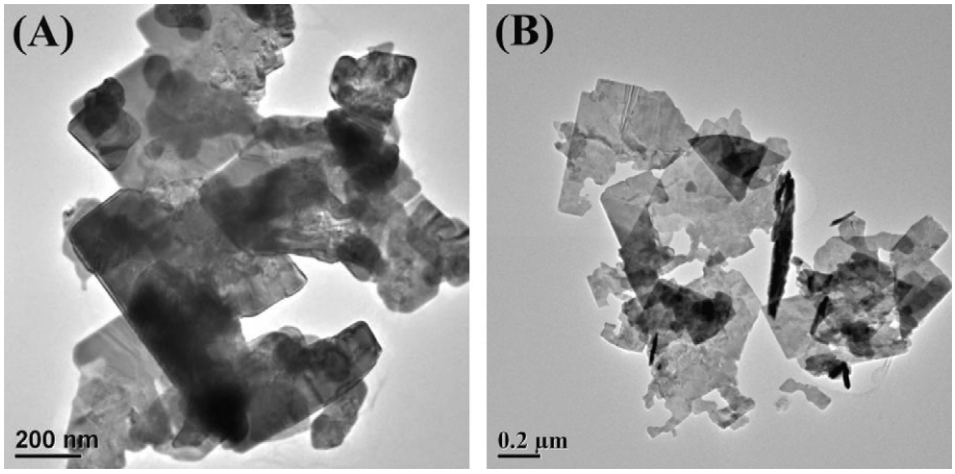

Fig. 2. TEM micrograph of (A) Zr-0 and (B) Zr-0.03.

of zirconium contents. The same results are also presented in other diffraction peaks. According to Bragg's law, $d_{(hkl)} = \lambda/(2\sin\theta)$, where $d_{(hkl)}$ is the distance between crystal planes of (hkl), λ is the X-ray wavelength, and θ is the diffraction angle of the crystal plane (hkl) [23], the decrease in 2θ value should result from the increase in lattice parameters ($d(1\,3\,1)$ value). Because the ionic radius of Zr^{4+} (0.080 nm) is smaller than that of Bi^{3+} (0.108 nm) but larger than that of W^{6+} (0.062 nm), the observed shift of diffraction peak toward lower angles should be due to the larger lattice parameter expected for substitution of W^{6+} by Zr^{4+}.

In order to obtain detailed information about the microstructure and morphology of the as-synthesized samples, TEM observations are carried out. Fig. 2(A) and (B) shows the representative TEM images of pure Bi_2WO_6 sample and Bi_2WO_6 sample doped with a zirconium content of 3.0 mol%, respectively. Both samples exhibit sheet-like morphology, which indicates that zirconium doping has no obvious influence on the morphology of Bi_2WO_6.

3.2. X-ray photoelectron spectroscopic (XPS) analysis

The surface composition and elementary oxidation states of the as-prepared sample with a zirconium content of 3.0 mol% is investigated using XPS analysis, and the corresponding experiment results are shown in Fig. 3. The overall XPS spectra shown in Fig. 3(A)

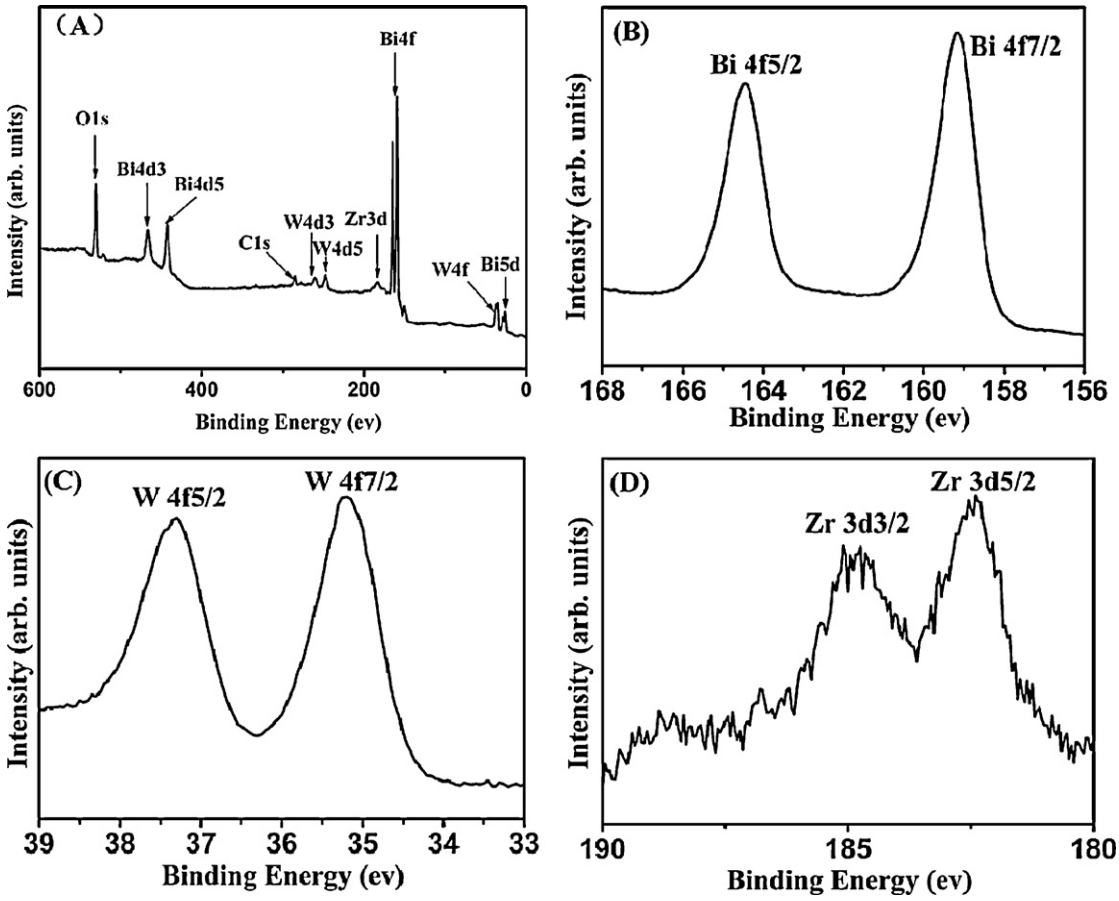

Fig. 3. XPS spectra of Zr-0.03. (A) The overall XPS spectra of the sample; (B) Bi 4f spectrum; (C) W 4f spectrum and (D) Zr 3d spectrum.

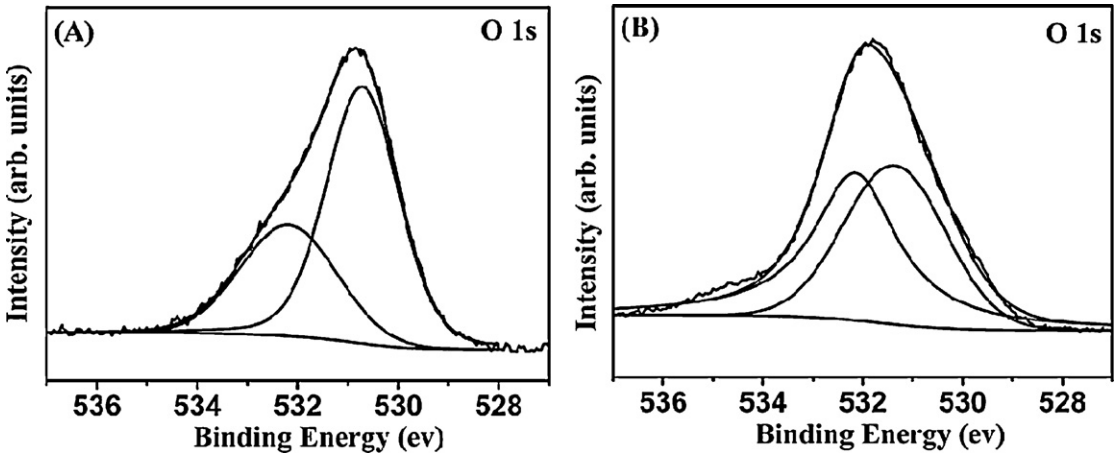

Fig. 4. High-resolution XPS spectra of O 1s for (A) Zr-0 and (B) Zr-0.03.

indicates that all of the peaks on the curve are ascribed to Bi, W, O, Zr and C elements and no peaks of other elements are observed. The presence of C comes mainly from carbon tape used for XPS measurement. Parts B–D of Fig. 3 display the high-resolution spectrum for Bi, W and Zr species, respectively. According to Fig. 3(B), the binding energies of Bi 4f7/2 and Bi 4f5/2 are 159.2 eV and 164.4 eV, respectively, which correspond to the characteristic peak of Bi^{3+}. The W 4f orbital is clearly resolved into W 4f5/2 and W 4f7/2 contributions, centered upon 37.3 eV and 35.2 eV, respectively (Fig. 3(C)), which are very close to previously reported values [19], suggesting that the tungsten in the Zr^{4+}-doped Bi_2WO_6 sample exists as W^{6+}. The Zr 3d spectra shown in Fig. 3(D) consists of Zr 3d3/2 and Zr 3d5/2 main peaks with a peak separation of 2.4 eV, which is in agreement with the literature data of Zr^{4+} [24].

Moreover, we investigated the presence of oxygen vacancies by the XPS spectra. The high-resolution O 1s XPS spectra of undoped Bi_2WO_6 and Zr^{4+}-doped Bi_2WO_6 samples were presented in Fig. 4(A) and (B), respectively. Both profiles are asymmetric and can be fitted to two Gaussian features, which are normally assigned as the low binding energy component (LBEC) and the high binding energy component (HBEC), indicating two different kinds of O species in the sample. The LBEC and HBEC can be attributed to the lattice oxygen and chemisorbed oxygen caused by the surface chemisorbed species such as hydroxyl and H_2O, respectively [25]. It has been previously reported that the HBEC component develops with the increase of oxygen vacancies [26], which can lead to the asymmetry of the main peak. The high-resolution O 1s XPS spectra indicate that the peak area of HBEC is obviously larger in the zirconium doped sample as compared to the undoped one. Moreover, the calculated ratios of the adsorbed oxygen to the lattice oxygen are 1.14 and 0.43 for the zirconium doped sample and undoped sample, respectively, which strongly suggests the presence of oxygen deficiencies in the zirconium doped sample.

3.3. Optical properties of the products

The UV–vis diffuse reflectance spectra (DRS) of Zr^{4+}-doped Bi_2WO_6 samples in comparison with pure Bi_2WO_6 are shown in Fig. 5. Pure Bi_2WO_6 sample presented the photoabsorption ability from the UV light region to the visible light with the wavelength shorter than 450 nm. It was noteworthy that the absorption onset of Zr^{4+}-doped Bi_2WO_6 samples was red-shifted apparently. With the increasing zirconium doping amount, the visible light absorption intensity of the samples became stronger, which may be attributed to excitations of trapped electrons in localized states associated with oxygen vacancies just below the conduction band minimum [27]. The oxygen vacancies are positive charges centers, which bound electrons easily. Excitation of the electrons from such local states to the conduction band can lead to better visible light absorbance. Therefore, with more zirconium dopant concentration, more oxygen vacancies are created, and optical absorption properties of the samples become stronger.

3.4. Photoluminescence spectra and photoelectrochemical measurements

Since photoluminescence (PL) emission mainly results from the recombination of free carriers, PL spectra is useful in determining the migration, transfer, and recombination processes of the photogenerated electron–hole pairs in a semiconductor. A weaker PL intensity implies a low recombination rate of the electron–hole under light irradiation [28]. Fig. 6(A) shows the PL spectra of undoped Bi_2WO_6 and Zr^{4+}-doped Bi_2WO_6 (Zr-0.03) when the excitation wavelength was 300 nm. There was a significant decrease in the intensity of PL spectra of Zr^{4+}-doped Bi_2WO_6, which confirmed that zirconium doping could effectively inhibit the recombination of photogenerated charge carriers.

Photocurrent reflects indirectly the semiconductor's ability to generate and transfer the photogenerated charge carriers, which correlates with the photocatalytic activity [29]. To investigate the photo-induced charges separation efficiency of undoped and zirconium doped samples, the photocurrent measurement was carried out under visible light irradiation. As shown in Fig. 6(B), the Zr-0.03 sample generates higher photocurrent than undoped Bi_2WO_6,

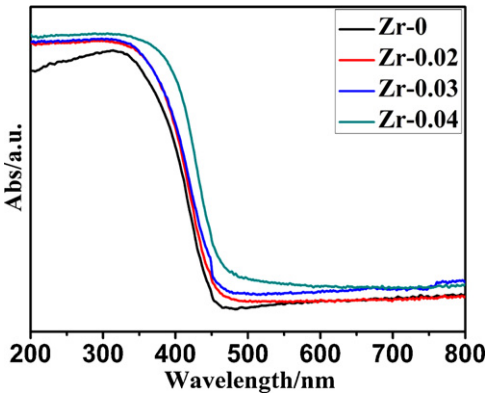

Fig. 5. UV–vis diffuse reflectance spectra of the as-prepared samples.

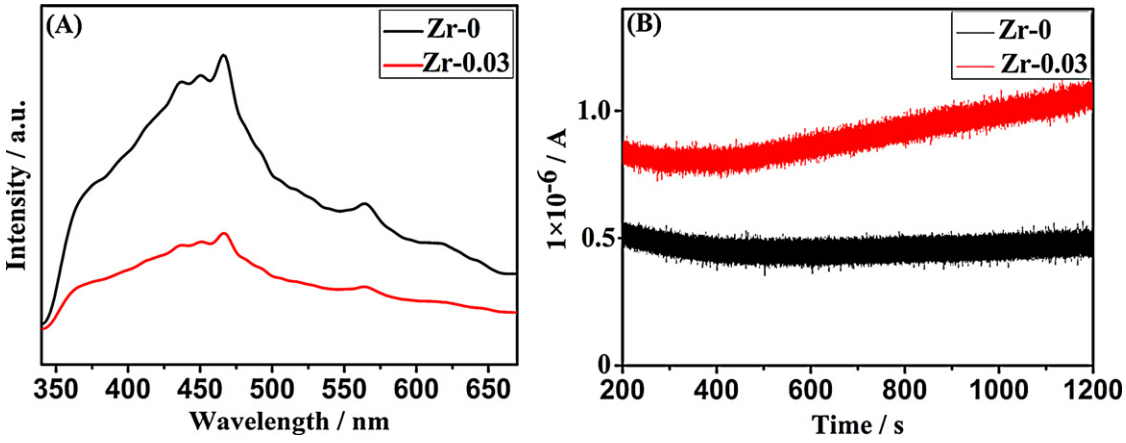

Fig. 6. (A) The room temperature photoluminescence (PL) spectrum of Zr-0.03 and Zr-0 (λ_{Ex} = 300 nm); (B) photocurrent generated with visible light irradiation time over Zr-0.03 and Zr-0 suspended with acetate and Fe^{3+}.

which indicates that zirconium doping can effectively promote the charge carrier transfer and reduce the electron–hole recombination.

3.5. Photocatalytic performance of Zr^{4+}-doped Bi_2WO_6 samples

RhB, a hazardous compound as well as a common model pollutant, was chosen as a representative pollutant to evaluate the photocatalytic performance of the photocatalysts. The RhB concentration variation versus the reaction time in the presence of Zr^{4+}-doped Bi_2WO_6 samples compared with pure Bi_2WO_6 is plotted in Fig. 7(A). The results demonstrate that the photoactivity of the samples was strongly dependent on the zirconium doping concentration. With zirconium concentration increasing from 0 mol% to 3.0 mol%, the photoactivity of the samples for the RhB photodegradation was enhanced. When the zirconium concentration increased to 4.0 mol%, the photoactivity decreased as compared to that of 3.0 mol%, but still higher than that of undoped Bi_2WO_6. The maximum photoactivity was observed for Zr-0.03, which can degrade RhB completely in 20 min, while only 65.4% of RhB was degraded in the presence of pure Bi_2WO_6 within the same time period. Moreover, the comparison of the apparent rate constant *k* in Fig. 7(B) demonstrated that Zr-0.03 had the highest *k* value in the photodegradation of RhB, while that of Zr-0.04 decreased compared with that of Zr-0.03. The reason can be interpreted as follows: appropriate amount of oxygen vacancies can trap the electrons, resulting in the holes free to diffuse to the semiconductor surface where oxidation of organic species can occur. Therefore, appropriate content of oxygen vacancies will improve the photocatalytic process by separating the electron–hole pairs effectively. If it exceeded the optimum value, however, the oxygen vacancies would act as the recombination centers for the photoinduced electrons and holes, which is unfavourable to the photocatalytic performance [27,30]. When the Zr doping concentration was 3.0 mol%, appropriate content of oxygen vacancies were generated and this photocatalyst exhibited the highest photocatalytic activity. When the doping concentration of Zr was increased further, the excess oxygen vacancies generated led to a poor photocatalytic performance. Therefore, appropriate zirconium doping amount can significantly enhance the photocatalytic activity of Bi_2WO_6.

Photocatalytic activities of the above-mentioned photocatalysts can be further tested by the degradation of some other organic compound, such as phenol that has no light absorption property in the visible light region and no photosensitization, as shown in Fig. 8. Obviously, upon visible-light irradiation, phenol is degraded more efficiently by Zr-0.03 than by pure Bi_2WO_6 (Fig. 8(A)). About 62.5% and 14.2% degradation efficiency was reached within 120 min by Zr-0.03 and pure Bi_2WO_6, respectively. In addition, due to pseudo-first-order kinetics of phenol photodegradation on Bi_2WO_6, the apparent rate constant k is calculated to be 0.0012 min^{-1} and 0.0083 min^{-1} for pure Bi_2WO_6 and Zr-0.03, respectively (Fig. 8(B)). In other words, the photocatalytic activity of Zr-0.03 is about 7 times that of pure Bi_2WO_6.

In order to further investigate the photodegradation of phenol, total organic carbon (TOC), which has been widely used to evaluate

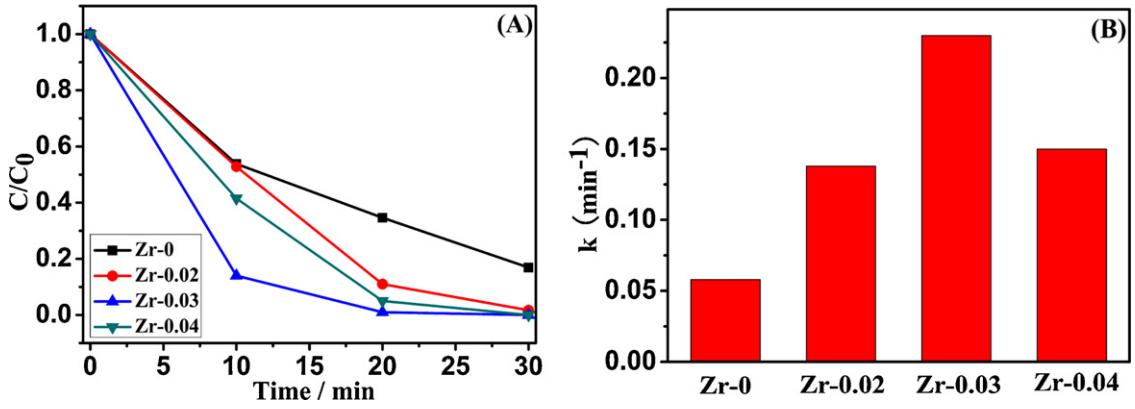

Fig. 7. (A) Photocatalytic degradation of RhB under visible light (λ > 420 nm) as a function of irradiation time by the as-prepared samples; (B) the comparison of rate constant *k*.

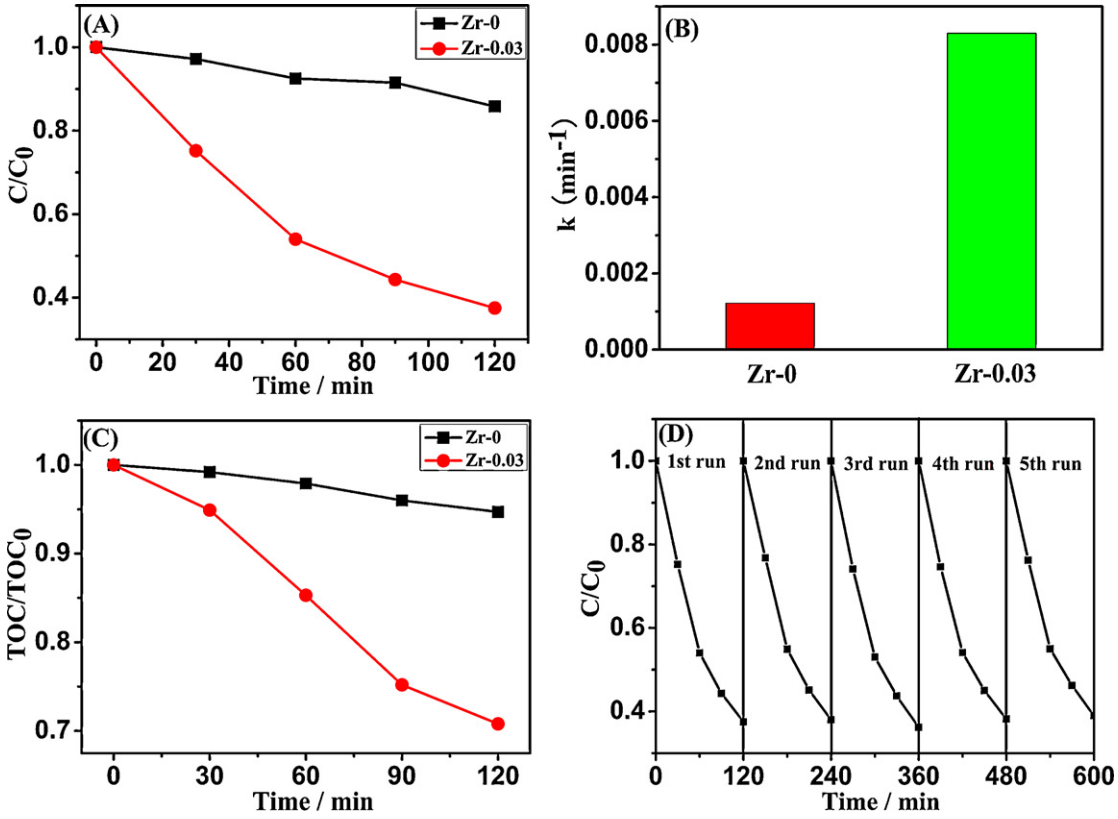

Fig. 8. (A) Photocatalytic degradation of phenol under visible-light irradiation by Zr-0.03 and Zr-0, respectively; (B) the comparison of rate constant *k*; (C) TOC removal efficiency during the course of photocatalytic degradation of phenol in the presence of Zr-0.03 and Zr-0, respectively; (D) cycling runs in the photocatalytic degradation of phenol under visible-light irradiation.

the degree of mineralization of organic species, was measured in the photodegradation process by the as-prepared samples under visible light, as shown in Fig. 8(C). The results confirm that phenol is steadily mineralized by the as-prepared samples. Moreover, the TOC removal efficiency in the presence of Zr-0.03 reaches a value of 29.2% after 120 min of irradiation, while that of Bi_2WO_6 is only 5.3%. Based on the above results, it can be deduced that Zr-0.03 is a much superior photocatalyst to pure Bi_2WO_6.

To check the stability of the Zr^{4+}-doped Bi_2WO_6 photocatalyst, the circulating runs in the photocatalytic degradation of phenol were performed under visible light. As shown in Fig. 8(D), after five recycles for the photodegradation of phenol, the catalyst did not exhibit any significant loss of activity, confirming the Zr^{4+}-doped Bi_2WO_6 is not photocorroded during the photocatalytic oxidation of the pollutant molecules, which is especially important for its application.

3.6. Mechanism of enhanced photoactivities

Photocatalysis generally involves four processes [31]: (i) light-induced generation of conduction band electrons and valence band holes; (ii) transfer of the photogenerated charge carriers to the photocatalyst surface; (iii) subsequent reduction/oxidization of the adsorbed reactants directly by electrons/holes or indirectly by reactive oxygen species; and (iv) recombination of the photogenerated electron–hole pairs. The photocatalysis efficiency is determined by the competition between the charge separation process and the charge recombination process. Desired photocatalysts are expected to promote the charge transfer processes while suppressing recombination process.

Typically, for photocatalysts in an aqueous solution, the photo-induced valence band holes can react with chemisorbed hydroxyl groups or H_2O to form surface-bound hydroxyl radicals (•OH) and the conduction band electrons can interact with adsorbed O_2 to form superoxide radicals ($O_2^{\bullet-}$), which are both strong oxidative species and play crucial roles in the oxidative degradation of organics [32,33]. However, for the Bi_2WO_6 system, the holes could not react with OH^-/H_2O to form •OH due to the more negative redox potential of Bi^V/Bi^{III} (+1.59 V) than that of $^\bullet OH/OH^-$ (+1.99 V) [34]. In order to ascertain the active species in the degradation process, holes and hydroxyl radicals scavengers were added into the degradation system. Fig. 9 showed that the addition of isopropanol (IPA) as hydroxyl radicals scavenger [34] caused a minor change in the photocatalytic degradation of phenol, indicating that •OH is not the major oxidation species in this process. However, when holes scavenger, EDTA [35] was introduced, the degradation rates of phenol

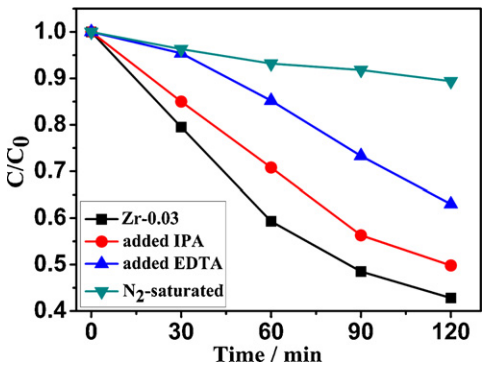

Fig. 9. Photocatalytic degradation of phenol with the addition of hole and hydroxyl radical scavengers and in N_2-saturated solutions under visible light irradiation ($\lambda > 420$ nm).

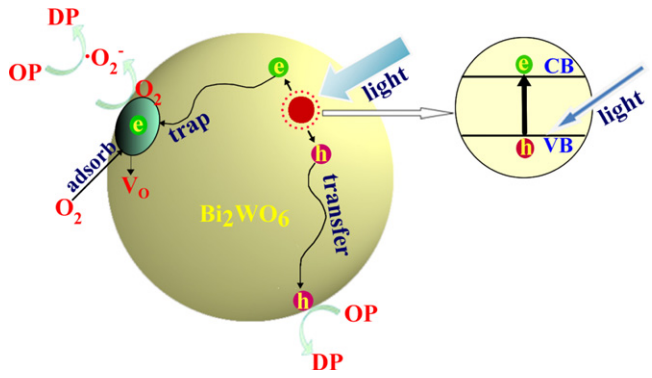

Fig. 10. Proposed photocatalytic mechanism of oxygen deficient Bi_2WO_6. OP: organic pollutant; DP: degradation product.

were depressed to a large extent. Therefore, holes play an important part in Bi_2WO_6 photocatalysis.

The superoxide radical is another important intermediate for oxidative degradation of organics [36,37]. In order to examine the role of superoxide radical in the photocatalysis, photocatalytic degradation of phenol was carried out under N_2-saturated conditions. The result shown in Fig. 9 indicated that under the anoxic condition, the photodegraded rate of phenol was largely suppressed, suggesting that superoxide radical is an important oxidation species in the photocatalytic process. Oxygen molecules as the electron scavengers play a crucial role in photocatalysis by reacting with electrons to generate superoxide radicals. However, when the rate of O_2 reduction by electrons is not sufficiently fast to match the rate of reaction of holes, an excess of electrons will accumulate on the photocatalyst particles, and the electron–hole recombination rate will increase consequently. In this case, electrons transfer to O_2 may be the rate limiting step in photocatalysis [38,39]. This, however, can be overcome by the introduction of oxygen vacancies into the photocatalyst.

In order to facilitate the reaction between oxygen and electrons, strong oxygen adsorption on the photocatalyst surface and longer lifetime of electrons are indispensable. It was reported that adsorption of O_2 molecules is mainly mediated by oxygen vacancies and oxygen physisorbs on defect-free oxide surfaces but interacts strongly with oxygen vacancies [40,41]. So the adsorption of oxygen can be promoted by the formation of oxygen vacancies. On the other hand, if an electron is freely mobile in the semiconductor particle, it is hardly possible for it to escape destiny of recombination. However, this can be prevented if the electrons are transiently but efficiently trapped in the particles. The positively charged $V_O^{\bullet\bullet}$ defects can work as electron acceptors and can trap the photogenerated electrons temporarily to reduce the surface recombination of electrons and holes [8,9]. Therefore, the creation of oxygen vacancies can not only favor oxygen adsorption but also retard the recombination of charge carriers, which facilitates the O_2 reduction rate to generate more superoxide anions ($O_2^{\bullet-}$) on the photocatalyst surface (Fig. 10), and thus lead to an enhanced photocatalytic activity.

4. Conclusions

Oxygen-deficient Bi_2WO_6 photocatalysts were synthesized by zirconium doping, and the relationship between oxygen vacancies and photocatalytic activities of Bi_2WO_6 was investigated. The visible-light-induced photo-degradation of RhB and phenol demonstrated that zirconium doping could significantly enhance the photocatalytic performance of Bi_2WO_6. The higher photocatalytic activity was attributed to the formation of oxygen vacancies, which promote the O_2 adsorption and O_2 reduction rate, leading to more superoxide anions on the photocatalyst surface. Generation of superoxide anions was a process of trapping the photoinduced electrons, which facilitated the charge separation and resulted in a lower electron–hole recombination rate. Our work suggests that the idea of oxygen vacancies introduction can be a plausible strategy to develop efficient visible-light-driven photocatalysts for environmental remediation.

Acknowledgements

We acknowledge the financial support from the National Natural Science Foundation of China (50972155, 50902144, 50732004), National Basic Research Program of China (2010CB933503) and Science Foundation for Youth Scholar of State Key Laboratory of High Performance Ceramics and Superfine Microstructures (SKL 200904).

References

[1] A.L. Linsebigler, G.Q. Lu, J.T. Yates, Photocatalysis on TiO_2 surfaces: principles mechanisms, and selected results, Chem. Rev. 95 (1995) 735–758.
[2] A. Hagfeldt, M. Gratzel, Light-induced redox reactions in nanocrystalline systems, Chem. Rev. 95 (1995) 49–68.
[3] X.B. Chen, S.S. Mao, Titanium dioxide nanomaterials: synthesis, properties, modifications, and applications, Chem. Rev. 107 (2007) 2891–2959.
[4] W. Morales, M. Cason, O. Aina, N.R. Tacconi, K. Rajeshwar, Combustion synthesis and characterization of nanocrystalline WO_3, J. Am. Chem. Soc. 130 (2008) 6318–6319.
[5] W.J. Youngblood, S.H.A. Lee, K. Maeda, T.E. Mallouk, Visible light water splitting using dye-sensitized oxide semiconductors, Acc. Chem. Res. 42 (2009) 1966–1973.
[6] M.R. Hoffmann, S.T. Martin, W.Y. Choi, D.W. Bahnemann, Environmental applications of semiconductor photocatalysis, Chem. Rev. 95 (1995) 69–96.
[7] T.J. Kuo, C.N. Lin, C.L. Kuo, M.H. Huang, Growth of ultralong ZnO nanowires on silicon substrates by vapor transport and their use as recyclable photocatalysts, Chem. Mater. 19 (2007) 5143–5147.
[8] J.C. Wang, P. Liu, X.Z. Fu, Z.H. Li, W. Han, X.X. Wang, Relationship between oxygen defects and the photocatalytic property of ZnO nanocrystals in nafion membranes, Langmuir 25 (2009) 1218–1223.
[9] Y.H. Zheng, C.Q. Chen, Y.Y. Zhan, X.Y. Lin, Q. Zheng, K.M. Wei, J.F. Zhu, Y.J. Zhu, Luminescence and photocatalytic activity of ZnO nanocrystals: correlation between structure and property, Inorg. Chem. 46 (2007) 6675–6682.
[10] X.Q. Gong, A. Selloni, M. Batzill, U. Diebold, Steps on anatase TiO_2 (1 0 1), Nat. Mater. 5 (2006) 665–670.
[11] A. Kudo, S. Hijii, H_2 or O_2 evolution from aqueous solutions on layered oxide photocatalysts consisting of Bi^{3+} with 6s2 configuration and d0 transition metal ions, Chem. Lett. 28 (1999) 1103–1104.
[12] C. Zhang, Y.F. Zhu, Synthesis of square Bi_2WO_6 nanoplates as high-activity visible-light-driven photocatalysts, Chem. Mater. 17 (2005) 3537–3545.
[13] H.B. Fu, L.W. Zhang, W.Q. Yao, Y.F. Zhu, Nanosized Bi_2WO_6 catalysts prepared by hydrothermal synthesis and their photocatalytic properties, Appl. Catal. B: Environ. 66 (2006) 100–110.
[14] F. Amano, A. Yamakata, K. Nogami, M. Osawa, B. Ohtani, Visible light responsive pristine metal oxide photocatalyst: enhancement of activity by crystallization under hydrothermal treatment, J. Am. Chem. Soc. 130 (2008) 17650–17651.
[15] G.S. Li, D.Q. Zhang, J.C. Yu, M.K.H. Leung, An efficient bismuth tungstate visible-light-driven photocatalyst for breaking down nitric oxide, Environ. Sci. Technol. 44 (2010) 4276–4281.
[16] J. Ren, W.Z. Wang, S.M. Sun, L. Zhang, J. Chang, Enhanced photocatalytic activity of Bi_2WO_6 loaded with Ag nanoparticles under visible light irradiation, Appl. Catal. B: Environ. 92 (2009) 50–55.
[17] Y.Y. Li, J.P. Liu, X.T. Huang, J.G. Yu, Carbon-modified Bi_2WO_6 nanostructures with improved photocatalytic activity under visible light, Dalton Trans. 39 (2010) 3420–3425.
[18] M. Shang, W.Z. Wang, L. Zhang, H.L. Xu, Bi_2WO_6 with significantly enhanced photocatalytic activities by nitrogen doping, Mater. Chem. Phys. 120 (2010) 155–159.
[19] Q. Xiao, J. Zhang, C. Xiao, X.K. Tan, Photocatalytic degradation of methylene blue over Co_3O_4/Bi_2WO_6 composite under visible light irradiation, Catal. Commun. 9 (2008) 1247–1253.
[20] L.S. Zhang, K.H. Wong, Z.G. Chen, J.C. Yu, J.C. Zhao, C. Hu, C.Y. Chan, P.K. Wong, AgBr–Ag–Bi_2WO_6 nanojunction system: a novel and efficient photocatalyst with double visible-light active components, Appl. Catal. A 363 (2009) 221–229.
[21] C.K. Lee, L.T. Sim, A.M. Coats, A.R. West, On possible Cu doping of Bi_2WO_6, J. Mater. Chem. 11 (2001) 1096–1099.
[22] M.S. Islam, S. Lazure, R.N. Vannier, G. Nowogrocki, G. Mairesse, Structural and computational studies of Bi_2WO_6 based oxygen ion conductors, J. Mater. Chem. 8 (1998) 655–660.
[23] G.L. Huang, Y.F. Zhu, Enhanced photocatalytic activity of $ZnWO_4$ catalyst via fluorine doping, J. Phys. Chem. C 111 (2007) 11952–11958.

[24] I. Atribak, A.B. Lopez, A.G. Garcia, B. Azambre, Contributions of surface and bulk heterogeneities to the NO oxidation activities of ceria–zirconia catalysts with composition $Ce_{0.76}Zr_{0.24}O_2$ prepared by different methods, Phys. Chem. Chem. Phys. 12 (2010) 13770–13779.
[25] Y.H. Zheng, L.R. Zheng, Y.Y. Zhan, X.Y. Lin, Q. Zheng, K.M. Wei, Ag/ZnO heterostructure nanocrystals: synthesis characterization and photocatalysis, Inorg. Chem. 46 (2007) 6980–6986.
[26] M. Naeem, S.K. Hasanain, M. Kobayashi, Y. Ishida, A. Fujimori, S. Buzby, S.I. Shah, Effect of reducing atmosphere on the magnetism of $Zn_{1-x}Co_xO$ ($0 \le x \le 0.10$) nanoparticles, Nanotechnology 17 (2006) 2675–2680.
[27] J. Wang, D.N. Tafen, J.P. Lewis, Z.L. Hong, A. Manivannan, M.J. Zhi, M. Li, Ni.Q. Wu, Origin of photocatalytic activity of nitrogen-doped TiO_2 nanobelts, J. Am. Chem. Soc. 131 (2009) 12290–12297.
[28] K. Fujihara, S. Izumi, T. Ohno, M. Matsumura, Time-resolved photoluminescence of particulate TiO_2 photocatalysts suspended in aqueous solutions, J. Photochem. Photobiol. A: Chem. 132 (2000) 99–104.
[29] H.G. Kim, P.H. Borse, W.Y. Choi, J.S. Lee, Photocatalytic nanodiodes for visible-light photocatalysis, Angew. Chem. Int. Ed. 44 (2005) 4585–4589.
[30] H.H. Wang, C.S. Xie, The effects of oxygen partial pressure on the microstructures and photocatalytic property of ZnO nanoparticles, Physica E 40 (2008) 2724–2729.
[31] N.Q. Wu, J. Wang, D.N. Tafen, H. Wang, J.G. Zheng, J.P. Lewis, X.G. Liu, S.S. Leonard, A. Manivannan, Shape-enhanced photocatalytic activity of single-crystalline anatase TiO_2 (1 0 1) nanobelts, J. Am. Chem. Soc. 132 (2010) 6679–6685.
[32] K. Ishibashi, A. Fujishima, T. Watanabe, K. Hashimoto, Generation and deactivation processes of superoxide formed on TiO_2 film illuminated by very weak UV light in air or water, J. Phys. Chem. B 104 (2000) 4934–4938.
[33] A.M. Peiro, C. Colombo, G. Doyle, J. Nelson, A. Mills, J.R. Durrant, Photochemical reduction of oxygen adsorbed to nanocrystalline TiO_2 films: a transient absorption and oxygen scavenging study of different TiO_2 preparations, J. Phys. Chem. B 110 (2006) 23255–23263.
[34] H.B. Fu, C.S. Pan, W.Q. Yao, Y.F. Zhu, Visible-light-induced degradation of rhodamine B by nanosized Bi_2WO_6, J. Phys. Chem. B 109 (2005) 22432–22439.
[35] F. Zhou, R. Shi, Y.F. Zhu, Significant enhancement of the visible photocatalytic degradation performances of γ-Bi_2MoO_6 nanoplate by graphene hybridization, J. Mol. Catal. A: Chem. 340 (2011) 77–82.
[36] S. Kim, H. Park, W. Choi, Comparative study of homogeneous and heterogeneous photocatalytic redox reactions: $PW_{12}O_{40}^{3-}$ vs. TiO_2, J. Phys. Chem. B 108 (2004) 6402–6411.
[37] L. Cermenati, P. Pichat, C. Guillard, A. Albini, Probing the TiO_2 photocatalytic mechanism in water purification by use of quinoline, photo-fenton generated OH radicals and superoxide dismutase, J. Phys. Chem. B 101 (1997) 2650–2658.
[38] C.M. Wang, A. Heller, H. Gerischer, Palladium catalysis of O_2 reduction by electrons accumulated on TiO_2 particles during photoassisted oxidation of organic compounds, J. Am. Chem. Soc. 114 (1992) 5230–5234.
[39] H. Gerischer, A. Heller, The role of oxygen in photooxidation of organic molecules on semiconductor particles, J. Phys. Chem. 95 (1991) 5261–5267.
[40] D. Pillay, Y. Wang, G.S. Hwang, Prediction of tetraoxygen formation on rutile TiO_2 (1 1 0), J. Am. Chem. Soc. 128 (2006) 14000–14001.
[41] G.A. Kimmel, N.G. Petrik, Tetraoxygen on reduced TiO_2(1 1 0): oxygen adsorption and reactions with bridging oxygen vacancies, Phys. Rev. Lett. 100 (2008) 196102.